ISSN: 2639-0108

Review Article

Advances in Theoretical & Computational Physics

Optical Transition Rates in a Cylindrical Quantum Wire with an Inverse Parabolic Potential

Moletlanyi Tshipa*[1] and Monkami Masale[2]

[1]*Department of Physics, University of Botswana, Gaborone, Botswana*

***Corresponding author**
Tshipa M, Department of Physics, University of Botswana, Private Bag 0022, Gaborone, Botswana. Tel: +267 3554711; Email: tshipam@mopipi.ub.bw

Submitted: 03 Apr 2019; **Accepted**: 22 Apr 2019; **Published**: 25 May 2019

Abstract

Electron transition rates due to interaction with circularly polarized light incident along the axis of a free-standing solid cylindrical nanowire are evaluated in the dipole approximation. In this case, the allowed optical transitions are only those for which the azimuthal quantum numbers of the initial and final states differ by unity. The envisaged electric potential of the quantum wire is modeled as inversely parabolic in the radial distance and such that it assumes a value of zero at the surface of the nanostructure. The investigations here are on the influence of this form of the confining potential on the transition rates involving some few electrons' states of higher radial quantum numbers, nonetheless limited to transitions only between a pair of the electron's energy sub bands. It is found that a sweep of the strength of the potential gives rise to modulations of the optical transition rates for higher radial quantum numbers. Furthermore, an increase of the strength of this potential reduces the transition energies thus such an increase redshifts peaks of the corresponding transitions rates.

Keywords: Optical Transition Rates, Cylindrical Quantum Wire, Electric Confining Potential

Introduction

Recent advances in nanotechnology have been rapid, and have led to the fabrication of nanostructures of different geometrical symmetry [1-4]. These quantum structures can be employed to realize a plethora of devices which utilize different properties of the quantum structures to perform various functions. The numerous device applications extend over a wide range of fields including biochemical sensing, medicine, energy generation and optoelectronics [5-11]. The celerity of operation and efficiencies of photonic devices, in particular, depend on optical transition rates of the constituent quantum structures. It is imperative, therefore, to build an understanding of their optical properties in order to optimize the performance of such nanodevices. Xu et al. studied transition rates for two dimensional quantum cascade lasers [12]. Optical transition rates were also studied in silicon nanostructures from photoluminescence measurements and in hexagonal nanowires [13, 14]. Studying transition rates is crucial also because they are indicative carrier lifetimes, which provides vital information with regards to carrier collection. For example, a wire-on-well nanostructure grown was shown to have enhanced carrier collection due to extended carrier lifetimes, or decreased transition rates [15]. In addition, quantum dots with different lifetimes have been utilized in cell imaging to obtain temporal and spectral resolution [16]. In this report, transition rates due to the interaction of electrons with circularly polarized radiation incident along the axis of a solid cylindrical nanowire are presented, within the dipole approximation framework. The novel feature of the system studied here is the confining potential of the quantum wire, which is modeled as inversely parabolic in the radial distance.

Theory

The system considered is a free-standing solid cylindrical nanowire of radius R and long length L_z with an intrinsic electric confinement potential modeled as follows,

$$V(\rho) = \begin{cases} \frac{1}{2}\mu\omega_0^2 R^2(R^2/\rho^2 - 1) \ldots\ldots \rho < R \\ \infty \ldots\ldots\ldots\ldots\ldots\ldots\ldots\ldots \rho \geq R \end{cases}, \quad (1)$$

Where μ is the effective electron mass and ω_0 is angular frequency associated with the classical harmonic oscillator. This form of a potential is very attractive due to its potential to model cylindrical and spherical quantum shells, as well as single-walled and multi-walled carbon nanotubes. In the effective-mass approximation and assuming cylindrical symmetry, the Schrödinger equation can be written as

$$-\frac{\hbar^2}{2\mu}\nabla^2\psi(\rho,z,\phi) + V(\rho)\psi(\rho,z,\phi) = E_T\psi(\rho,z,\phi), \quad (2)$$

Where $\hbar = h/2\pi$, in which h is Planck's constant and E_T the total energy of the electron. The Schrödinger equation above is separable hence the electron's wave function $\psi(\rho, z, \phi)$ is sought in the general form

$$\psi(\rho,z,\phi) = C_{ml}\chi_{ml}(\rho)e^{ik_z z}e^{im\phi}, \quad (3)$$

Where C_{ml} is the normalization constant, indexed by the azimuthal and radial quantum numbers, m and l, respectively, where as k_z is the axial wave number of the electron. The radial part of the total electron's wave function satisfies the following differential equation:

$$\frac{1}{\rho}\frac{d}{d\rho}\left(\rho\frac{d}{d}\chi(\rho)\right) + \left[\frac{2\mu}{\hbar^2}\left(E_{ml} + \frac{1}{2}\mu\omega_0^2R^2\right) - \frac{1}{\rho^2}(m^2 + \mu^2\omega_0^2R^4/\hbar^2)\right]\chi(\rho) = 0 \quad (4)$$

Where E_{ml} is the electron's confinement sub band energy eigenvalue. The differential equation for χ satisfies Bessel's equation of fractional order ν, thence the complete solution of which is a linear combination of the $J_{\nu l}$ and $Y_{\nu l}$ Bessel functions [17]. The function Y, however, diverges at the origin and is therefore discarded as a solution in a solid cylindrical quantum wire. Thus, the solution of the Schrödinger equation that is well behaved in the region of the solid cylindrical quantum wire is taken as

$$\psi(\rho,z,\phi) = J_{\nu l}(\kappa\rho)e^{ik_z z}e^{im\phi} \quad (5)$$

Where $\kappa = \sqrt{2\mu\left(E_{ml} + \frac{1}{2}\mu\omega_0^2R^2\right)/\hbar^2}$ and

$\nu = \sqrt{m^2 + (\mu^2\omega_0^2R^4)/\hbar^2}$. The application of the standard boundary condition that the electron's wave function must vanish at the walls of the cylinder ($\rho = R$) leads to the following eigenvalue equation $J_{\nu l}(\kappa R) = 0$. The electron's energy spectrum can then be mapped out according to

$$E_T = E_{ml} + \frac{\hbar^2k_z^2}{2\mu} = \frac{\hbar^2 j_{\nu l}^2}{2\mu R^2} - \frac{1}{2}\mu\omega_0^2R^2 + \frac{\hbar^2k_z^2}{2\mu} \quad (6)$$

in which $j_{\nu l}$ is the lth root of the νth Bessel function $J_{\nu l}(\varsigma)$.

Transition rates

The two rudimentary processes of optical transitions considered here are that of absorption or stimulated emission of a photon by an electron. In these processes, an electron in an initial state $\{m,l\}$ can emit or absorb electromagnetic radiation of energy equal to $\hbar\omega$ and thereby make a transition to the final state $\{m', l'\}$. Such a transition is accompanied by a change of the electron's energy, nonetheless, such that the total energy is conserved according to: $\Delta E = |Em'l' - Eml| = \hbar\omega$. The transition rate from an initial state ψ_i with energy E_i to a final state ψ_f with energy E_f of the electron is given by the Fermi Golden rule [18].

$$W_{fi} = \frac{2\mu}{\hbar^2}\left|< \psi_f|H_{int}|\psi_i >\right|^2\delta(E_f - E_i \pm \hbar\omega). \quad (7)$$

The electron-photon interaction H_{int} is given by

$$H_{int} = -\frac{e}{\mu}\mathbf{A_\omega}\cdot\mathbf{p}$$

$$= -\frac{e}{2\mu}A_0\left[e^{i(\mathbf{q}\cdot\mathbf{r}-\omega t)} + e^{-i(\mathbf{q}\cdot\mathbf{r}-\omega t)}\right]\hat{\epsilon}\cdot\mathbf{p}$$

where $\mathbf{q}$ the photon field wave vector, $\mathbf{r}$ the electron position vector, $\hat{\epsilon}$ is the unitary polarization vector of the radiation field and A_0 is the amplitude of the vector potential. The amplitude of the vector potential can be written as

$$A_0 = \sqrt{(N_q\hbar)/(2\epsilon_0\epsilon_m\omega V)},$$

where N_q is the number of photons in volume V of the wire of dielectric constant ϵ_m and ϵ_0 is the permittivity of free space. Now, for circularly polarized light incident along the axis of the core, $\mathbf{q} = (0,0,q_z)$ and $\hat{\epsilon}\cdot\mathbf{p} = \rho(cos\phi \pm sin\phi)$, where the + (-) is for right (left) circular polarization. The matrix elements are evaluated as follows

$$< \psi_f|H_{int}|\psi_i >= \frac{eA_0}{2\mu} < \psi_f|e^{i\mathbf{q}\cdot\mathbf{r}}\hat{\epsilon}\cdot\mathbf{p}|\psi_i > \quad (8)$$

$$= \frac{eA_0}{iV\hbar}(E_f - E_i)RI_{m\prime l\prime ml}\delta_{k_z - k'_z \pm q_z,0}\delta_{m-m\prime\pm1,0}$$

where

$$I_{m\prime l\prime ml} = \int_0^1 x^2\ \chi_{m\prime l\prime}(x)\chi_{ml}(x)dx, \quad (9)$$

is the so-called interaction integral and $x=\rho/R$. In the last expression, the identity: $\mathbf{p}= [\mu(E_f - E_i)\mathrm{r}]/(i\hbar)$, in the Heisenberg equations of motion for operators, has been used [19]. The Kronecker delta: $\delta k_z - k'_z \pm q_z,0$ in equation means that the respective axial wave numbers are related according to $k'_z = k_z \pm q_z$, which is simply a statement of conservation of axial linear momentum [8]. The emergence of the Kronecker delta: $\delta_{m-m'\pm1,0}$ in equation is rather interesting in that it is a mathematical statement of the selection rules for the optical transitions considered here [8]. For circularly polarized light and in the dipole approximation, the only allowed optical transitions are those for which the azimuthal quantum numbers of the initial and the final states differ by unity. These selection rules of optical transitions apply only to the azimuthal quantum numbers and with no restriction on the radial quantum numbers. For an electron wave function of the form given in Eq, the transition rates are found to be [20, 21].

$$W_{fi} = W_0 I^2_{m\prime l\prime ml}\delta(E_f - E_i \pm \hbar\omega) \quad (10)$$

where $W_0 = n_z e^2\left(E_f - E_i\right)^2/(\epsilon_0\epsilon_m\hbar^2\omega)$, with n_z being photon linear density. The absorption and the emission transition rates, respectively, are explicitly given by

$$W^{abs}_{fi} = W_0 I^2_{m\prime l\prime ml}\delta(E_f - E_i - \hbar\omega) \quad (11)$$

and

$$W^{em}_{fi} = W_0 I^2_{m\prime l\prime ml}\delta(E_f - E_i + \hbar\omega) \quad (12)$$

Finally, it is helpful especially for purposes of computation, to replace the Dirac delta function with a Lorentzian factor according to

$$\delta(E_f - E_i + \hbar\omega) \to \frac{\gamma}{\pi(E_f - E_i \pm \hbar\omega)^2 + \gamma^2},$$

in which γ is the so-called linewidth of resonance. The actual total transition rate of the quantum system involves a summation of all

the individual transition rates, of course, taking into account the transition probabilities of all the allowed transitions.

Results and discussions

The key relevant parameters used in the computations here are μ=0.067m_e, where m_e is free-mass of the electron and ϵ_m=12.5, pertaining to GaAs crystals. The linewidth has been taken as γ=5 meV and n_z=2.895×10^7/m. The functional forms of the emission and absorption optical transition rates are very similar hence, for brevity, only the results for the absorption process are shown.

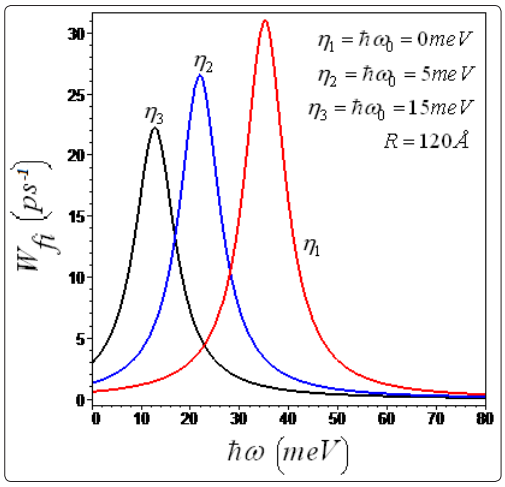

Figure 1: The (m=0→m'=1,l=l'=1) optical transition rates as functions of the photon energy in a cylindrical nanowire of radius R=120Å and with an inverse parabolic potential of strengths: η_1=$\hbar\omega_0$=0 meV, η_2=$\hbar\omega_0$=5 meV and η_3=$\hbar\omega_0$=15 meV

Figure 1 depicts the (m=0→m'=1, l=l'=1) absorption transition rates as functions of the photon energy in a cylindrical nanowire of radius R=120Å for some few different values of the strength of the inverse parabolic potential; viz: η_1=$\hbar\omega_0$=0 meV, η_2=$\hbar\omega_0$=5 meV and η_3=$\hbar\omega_0$=15 meV, as indicated. Each curve of the l=l'=1 transition rate is characterized by a resonance peak in its variation with the photon energy. Typically, resonance peaks of optical transition rates occur whenever the electron's energy subband separations of the states involved exactly match the photon energy. Just like in resonance behavior of a forced simple harmonic oscillator, the width of the resonance peak is determined by the line-width of resonance. It is also seen from figure 1 that these resonance peaks shift to lower values of the photon energy as the strength of the potential is increased. This is because the energy separations between the subbands involved here decrease as the strength of the potential is increased. It is interesting to note that this form of the potential, in a sense, imparts some fractional angular momentum to the electron. In particular, for finite values of $\hbar\omega_0$, the m=0 subband no longer possesses zero angular momentum. This effect has a bearing on the phase of the electron's wave functions across the radius of the cylindrical quantum wire. These results compare well with the experimental results of radiative lifetimes of excitons in quantum GaAs wires, which are of the order of picoseconds [22].

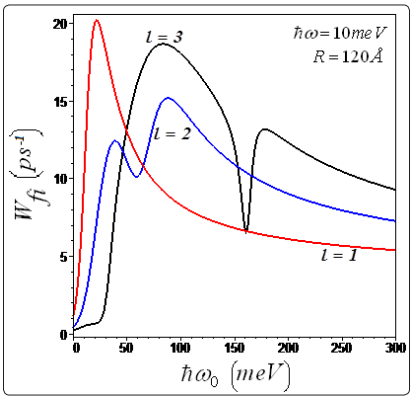

Figure 2: The variation of optical transition rates (from the m=0 state to the m'=1 state) with strength of the inverse parabolic potential for radial quantum numbers l=l'=1,2 and 3, in a cylindrical quantum wire of radius R=120Å. The energy of the incident radiation $\hbar\omega$=10 meV

Figure 2 depicts the (m=0→m'=1) optical transition rates as functions of strength of the inverse parabolic potential in a cylindrical wire of radius R=120Å, and at $\hbar\omega$=10 meV, for some few values of the radial quantum numbers l=l'=1,2 and 3, as indicated. Just like in figure 1, the curve for l=l'=1 transition rate is characterized by a single resonance peak in its variation with the strength of the potential. The curves for the transition rates corresponding to higher radial quantum numbers, however, exhibit multiple phase changes in their variations with $\hbar\omega$0. This behavior of the l>1 transition rates is closely related to the phase changes of the corresponding electron's wavefunctions across the radius of the wire, as $\hbar\omega$0 is varied. Recall that the electron's radial wavefunctions mimic standing waves of a string, with l essentially a count of the nodes of the wavefunctions. Now, the nature of the inverse parabolic potential is such that it "expels" electrons away from the axis of the wire, towards the walls of the quantum wire. This is signified by the shifting of peaks of electron's wave functions away from the wire axis as $\hbar\omega_0$ is increased. These phase changes of the wavefunctions are then reflected in the behavior of the transition rates in their variation with $\hbar\omega_0$, through the interaction integral. Arguably, the occurrence of minima or `secondary' maxima of the transition rates in their variation with $\hbar\omega_0$ is a manifestation of the degree of overlap between the electron's wavefunctions of the initial and final states.

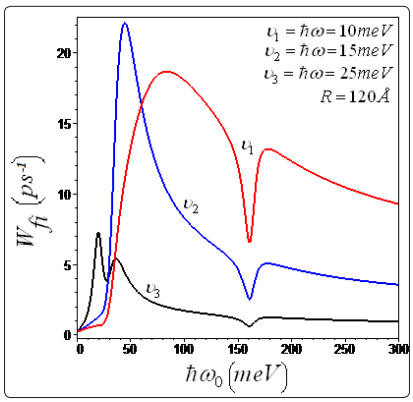

Figure 3: The (m=0→m'=1,l=l'=3) optical transition rates as functions of strength of the inverse parabolic potential in a cylindrical nanowire of radius R=120Å for radiation field energies υ_1=$\hbar\omega$=10 meV, υ_2=$\hbar\omega$=15 meV and υ_3=$\hbar\omega$=25 meV

Figure 3 shows the variation of the (m=0→m'=1,l=l'=3) optical transition rates with strength of the inverse parabolic potential in a cylindrical nanowire of radius R=120Å, for different energies of the photon field: υ_1=$\hbar\omega$=10 meV, υ_2=$\hbar\omega$=15 meV and υ_3=$\hbar\omega$=25 meV. Again, apart from the anticipated resonance peak, each curve of the transition rate possesses `secondary' maxima and minima in its variations with $\hbar\omega_0$. As mentioned earlier, this is indicative of the degree of coherence of the electron-photon interactions, as will be reflected in the behavior of the interaction integral in its variation with the strength of this potential [17]. Overall, the transition rates are lower for higher photon energies. This is because the corresponding electron's energy separations decrease with the increase of the strength of this potential.

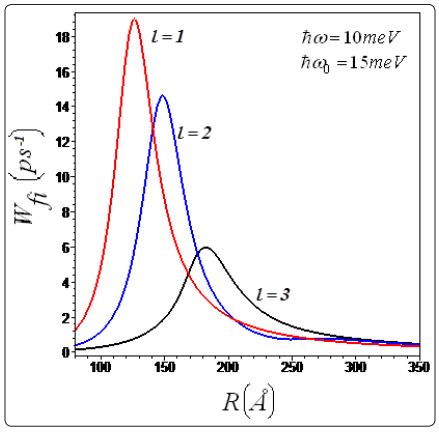

Figure 4: The variations of the (m=0→m'=1) transition rates with the radius of the nanowire for some few radial quantum numbers; viz; l=l'=1,2 and 3, as indicated. The other relevant parameters are $\hbar\omega$=10 meV and $\hbar\omega_0$=15 meV.

Figure 4 shows the variations of the (m=0→m'=1) transition rates with the radius of the nanowire for some few radial quantum numbers; viz; l=l'=1,2 and 3, as indicated. The other relevant parameters are $\hbar\omega$=10 meV and $\hbar\omega_0$=15 meV. It is seen that the resonance peaks corresponding to lower radial quantum numbers systematically occur at lower values of the radius of the cylindrical wire. The transitions are stronger for lower radial quantum number states due to prominent phase changes of the corresponding eigenfunctions. Furthermore, the electron's energy subband separations are relatively larger for higher radial quantum numbers.

Conclusions

Optical transition rates of a solid cylindrical wire were evaluated as functions of the inverse parabolic electric potential of the wire within the dipole approximation. The classical radiation field was taken to be that of circularly polarized light incident along the axis of the wire. For circularly polarized light and in the dipole approximation, the allowed transitions are only those for which the azimuthal quantum numbers of the initial and final electron's states differ by unity. As anticipated, stronger transitions were found for lower rather than higher radial quantum numbers of the electron's eigenfunctions. This is because the phase changes of the electron's eigenfunctions across the nanostructure are more pronounced for higher radial quantum numbers. This effect subsequently results in relatively lower values of the interaction integral hence lower values of the corresponding transition rates. The results shown also suggest that these transitions are weaker for greater values of the strength of the electric potential. The reason for this effect is twofold. First, an increase of the strength of this potential leads to more pronounced relative phase shifts of the electron's eigenfunctions across the radius of the wire. Second, the electron's subband energy separations decrease with the increase of the strength of this electric potential. This is particularly so here, in the case of a free standing cylindrical quantum wire. Finally, inherent in the reduction of the phase-space for the motion of the charge carriers, the transition rates become more enhanced as the radius of the quantum wire is decreased.

References

1. Gunawidjaja R, Diez-y Riega H, Eilers H (2015) Synthesis and characterizations of spherical Eu: La2O3 and related core/shell nanoparticles. Powder Technol. 271: 255-261.
2. Kontopoulou I, Angelopoulou A, Bouropoulos N (2016) ZnO spherical porous nanostructures obtained by thermal decomposition of zinc palmitate. Mater Lett 165: 87-90.
3. Zhong B, Zu X, Yi G, Huang H, Zhang M, et al. (2016) Fluorescence enhancement of the conjugated polymer films based on well-ordered Au nanoparticle arrays. J Nanopart Res 18: 281.
4. Liu Y, Zhou Y, Yang L, Wang Y, Wu Y, et al. (2016) Hydrothermal synthesis of 3D urchin-like Ag/TiO2/reduced graphene oxide composites and its enhanced photo catalytic performance. J Nanopart Res 18: 283.
5. Walmsley GG, McArdle A, Tevlin R, Momeni A, Atashroo D, et al. (2015) Nanotechnology in bone tissue engineering. Nanomed-Nanotechnol 11: 1253-1263.
6. Shi Y, Guo H, Yang J, Zhao M, Liu J, Xue C, et al. (2015) Plasma-Induced Wafer-Scale Self-Assembly of Silver Nanoparticles and Application to Biochemical Sensing. Materials 8: 3806-3814.
7. Shi F, Zhang Y, Yang G, Guo T, Feng N (2015) Preparation of a micro/nanotechnology based multi-unit drug delivery system for a Chinese medicine Niuhuang Xingxiao Wan and assessment of its antitumor efficacy. Int J Pharm 492: 244-247.
8. Irawan D, Saktioto T, Ali J, Yupapin P (2015) Design of Mach-Zehnder Interferometer and Ring Resonator for Biochemical Sensing. Photonic Sensors 5: 12-18.
9. Sirelkhatim A, Mahmud S, Seeni A, Kaus NHM (2016) Preferential cytotoxicity of ZnO nanoparticle towards cervical cancer cells induced by ROS-mediated apoptosis and cell cycle arrest for cancer therapy. J Nanopart Res 18: 219.
10. Mo L, Yang L, Lee ElH, He S (2015) High-efficiency plasmonic metamaterial selective emitter based on an optimized spherical core-shell nanostructure for planar solar thermophotovoltaics. Plasmonics 10: 529-538.
11. Najafi F, Dane A, Bellei F, Zhao Q, Sunter KA, et al. (2015) Fabrication process yielding saturated nanowire single-photon detectors with 24-ps jitter. IEEE J Sel Top Quant 21: 3800507.
12. Xu J, Liu L, Li BH, Zhang Z, Ma J, et al. (2016) Quantum cascade lasers designed toward shorter wavelengths. J Phys: Condens Matter 28: 065302.
13. Sangghaleh F, Sychugov I, Yang Z, Veinot JGC (2015) Near-unity internal quantum efficiency of luminescent Silicon nanocrystals with ligand passivation. ACS Nano 9: 7097-7104.
14. Chimalgi VU, Nishat MdRK, Ahmed SS (2015) nonlinear polarization and efficiency droop in hexagonal In GaN/GaN disk-in-wire LEDs. Superlattice Microst 84: 91-98.
15. Sugiyama M, Fujii H, Katoh T, Toprasertpong K, Sodabanlu H, et al. (2016) Quantum wire-on-well (Wow) cell with long carrier lifetime for efficient carrier transport. Prog Photovolt Res Appl 24: 1606-1614.

16. Zhang B, Yang C, Gao Y, Wang Y, Bu C, et al. (2017) Engineering quantum dots with different emission wavelengths and specific fluorescence lifetimes for spectrally and temporally multiplexed imaging of cells, Nanotheranostics 1: 131-140.
17. Tshipa M (2014) Oscillator strength for optical transitions in a cylindrical quantum wire with an inverse parabolic confining electric potential. Indian J Phys 88: 849-853.
18. Hashimzade FM, Ismailov TG, Mehdiyev BH (2005) Influence of external transverse electric and magnetic fields on the absorption of a parabolic quantum wire. Physica E 27: 140-150.
19. Scully MO, Zubairy MS (1997) Quantum Optics (Cambridge University Press).
20. Nag BR (2000) Physics of Quantum Well Devices (Kluwer Academic Publishers).
21. Ridley BK (1999) Quantum Processes in Semiconductors (Oxford University Press).
22. Kono T, Tsukamoto S, Nagamune Y, Sogawa F, Nishioka M, et al. (1994) Exciton radiative lifetime in GaAs quantum wires grown by metalorganic chemical-vapor selective growth. Appl Phys Lett 64: 1564-1566.